CEEMDAN-based Single-Channel Blind Source Extraction for Bearing Fault Detection and Diagnosis

Yuan Xie, Zhangchi Wei, Jinshi Yu, Yifei Sun, and Zhipeng Chen

***Abstract*—*Introduction*: Bearings are key components for power transmission in industrial applications. However, how to accurately detect bearing status and perform fault diagnosis in intense background noise remains a challenging task. *Methodology*: This paper presents a single-channel blind extraction algorithm for bearing fault detection and diagnosis. First, the vibration signal is decomposed into several intrinsic model functions (IMFs) and a residual. Using a kurtosis index technique to filter the decomposed IMF components, thereby building a multi-channel feature set and overcoming the problem of mode mixing. Then, a blind extraction technology is used to extract fault features from the virtual multi-channel mixed signals. Furthermore, the maximum energy amplitude at the fault feature frequency is obtained to identify fault features by using envelope spectrum analysis. Finally, determining the type of fault in the bearing through the magnitude of singular value entropy to achieve fault diagnosis. *Results*: The proposed algorithm can make the pulse component in the measurement signal more prominent and suppress the noise component entirely, achieving a powerful de-noising ability. Compared to the best comparison algorithm in this paper, the signal-to-noise ratio has been increased by a maximum of 53.35%, and the root mean square error has been decreased by a maximum of 10.86%. *Conclusion*: Experimental results based on the public bearing fault signal datasets verify the feasibility and superiority. The proposed algorithm constructs a complete automated diagnostic chain from signal denoising to state evaluation, and then to fault localization and diagnosis, which helps to diagnose bearing faults in practical industrial application scenarios.**

Link to graphical and video abstracts, and to code:
https://latamt.ieeer9.org/index.php/transactions/article/view/10347

***Index Terms*—Bearing fault diagnosis, blind source extraction, Hilbert envelope spectrum analysis, singular value entropy.**

I. Introduction

THE operational state of bearings, being essential transmission components, is a key factor for the safety of mechanical equipment. Bearing fault detection and diagnosis are crucial to ensure the regular operation of equipment and maintaining production efficiency [1], [2]. Owing to their inherent complexity and the presence of strong background noise in severe operational environments, bearing vibration signals often have weak fault features that are easily concealed, thereby impeding accurate detection and diagnosis Thus, the denoising and reconstruction process of standard signals is critical in the fault diagnosis process.

Blind source separation (BSS) technology can extract fault characteristic signals from noisy mixed signals, providing a foundation for subsequent fault diagnosis [3], [4]. When a composite fault occurs, the signals generated by different fault sources become mixed, increasing the difficulty of diagnosis. BSS can decompose these mixed signals into independent signal sources and separate the characteristic signals corresponding to various faults, thereby achieving accurate diagnosis of multiple faults. Blind source extraction (BSE) refers to extracting one or more sources of interest from the mixed signals [5], [6]. It is an extension of BSS [7], [8].

Because BSE does not require prior knowledge of fault characteristic frequencies or noise statistical characteristics, it can separate source signals based solely on the assumption of statistical independence of the signals, making it suitable for scenarios with complex noise and unknown fault modes in actual working conditions. Blind extraction technology can effectively extract specific frequency impact signals to determine the fault type and location when bearing faults occur. The independent fault signals obtained through blind extraction have more obvious and prominent features, which can be further enhanced by envelope demodulation and fast spectrum correlation [9]. However, in a single sensor scenario, the information contained in a single observation signal is much smaller than the amount of information that needs to be recovered from multiple source signals [10], [11]. In addition, the single-channel blind extraction is a pathological inverse problem with no unique solution and extremely ill-conditioned.

Empirical mode decomposition (EMD) decomposes a single channel vibration signal into multiple intrinsic model function (IMF) components [12], [13]. The decomposed IMFs are reconstructed to build a multi-channel mixed signals, which is then input into a fast independent component analysis algorithm to realize independent separation of fault signals [14]. However, EMD technology has a remarkable shortcoming of "mode mixing", as IMF contains similar oscillations between different modes, resulting in mixing. Therefore, the ensemble EMD (EEMD) and complete EEMD with adaptive noise (CEEMDAN) were presented [15], [16]. The CEEMDAN achieved negligible reconstruction errors and solved the mode

The associate editor coordinating the review of this manuscript and approving it for publication was Guillermo Valencia-Palomo (*Corresponding author: Zhangchi Wei*).

This work was mainly funded by the National Science Foundation of China (52305458), Wuzhou Science and Technology Plan Project (202502014).

Y. Xie, Zhangchi Wei, J. Yu, Y. Sun, and Z. Chen are with the School of Mechanical and Electrical Engineering, Guangzhou University, Guangzhou, 510006, China (e-mails: xieyuan@gzhu.edu.cn, wzc123@e.gzhu.edu.cn, jinshi.yu@gzhu.edu.cn, asunyifei@gzhu.edu.cn, and chenzhipeng@gzhu.edu.cn).

quantity variation under different implementation methods of signal plus noise, which had been applied in biomedical engineering [17], [18], noise reduction [19], [20], and rolling bearing fault diagnosis [21], [22]. However, these methods have limitations in fault detection and diagnosis in strong noise signal environments.

To detect and diagnose early bearing faults using weak signals in strong background noise signal conditions, a CEEMDAN-based single-channel blind source extraction algorithm, abbreviated as CEEMDAN-SCBSE, is proposed. First, the single-channel bearing vibration signal is decomposed into several IMFs and a residual by using the CEEMDAN. Second, the kurtosis of each IMF is calculated using the kurtosis criterion to select the IMFs that contain more fault features. Third, reconstructing the decomposed IMF components into multiple-channel signals, thereby achieving fault feature extraction of the signal via the BSE algorithm. Then, using envelope spectrum analysis to obtain the maximum energy amplitude at the fault feature frequency makes it easy to identify fault features. Finally, the fault type is determined using an information entropy technology. The flowchart is shown in Fig. 1.

The main novelty is as follows:

- A CEEMDAN-SCBSE algorithm is presented for bearing fault detection and diagnosis, facilitating accurate identification of fault features and eliminating noise interference.
- The proposed algorithm enables the maximum energy amplitude to be located at the fault feature frequency, making it easy to identify and capable of identifying multiple harmonics, and the singular value entropy of specific fault signals can be stably maintained within a certain range, making it easy to detect and diagnose.
- The feasibility and generalization ability of the CEEMDAN-SCBSE in engineering are verified by taking the bearing fault signals as examples. In addition, the proposed algorithm demonstrates excellent noise reduction capability.

II. Methodology

A. CEEMDAN Decomposition

CEEMDAN is a commonly used signal decomposition method in time series prediction, capable of effectively decomposing the original signal sequence into its constituent components. It addresses the mode-mixing and superposition issues encountered in EMD, thereby reducing the number of iterations and computational workload. The steps of CEEMDAN decomposition are as:

1) Let the vibration signal be $x(t)$. Set the noise amplitude ϵ_n that is typically a multiple of the standard deviation of the signal, and N is the total number of iterations. Initialize the residual $r_0(t) = x(t)$.

2) In the nth iteration, generate a set of Gaussian white noise $w_n(t)$ with ϵ_i. Add the noise to the current residual $r_{n-1}(t)$ to get the noisy signal:

$$x_1^n(t) = r_0(t) + \epsilon_i \cdot w_n(t). \tag{1}$$

3) The noisy signal $x_1^n(t)$ is subjected to EMD decomposition to acquire the first modal component $\text{IMF}_1^n(t)$ and the residual $r_n(t)$:

$$x_1^n(t) = \text{IMF}_1^n(t) + r_n(t). \tag{2}$$

Save $\text{IMF}_1^n(t)$ as the first modal component of the nth iteration.

4) Integrate the results of all iterations to calculate the first overall modal component $\text{IMF}_1(t)$:

$$\text{IMF}_1(t) = \frac{1}{N}\sum_{n=1}^{N} \text{IMF}_1^n(t), \tag{3}$$

and the residual is updated:

$$r_1(t) = x(t) - \text{IMF}_1(t). \tag{4}$$

5) For the jth modal component ($j \geq 2$) repeat the following steps:

a) Add extra noise to the current residual $r_{j-1}(t)$:

$$x_j^n(t) = r_{j-1}(t) + \epsilon_i \cdot w_n(t). \tag{5}$$

b) The noisy signal $x_j^n(t)$ is subjected to EMD decomposition to acquire the jth modal component $IMF_j^n(t)$ and the residual $r_j^n(t)$:

$$x_j^n(t) = \text{IMF}_j^n(t) + r_j^n(t). \tag{6}$$

c) Calculate the jth overall modal component:

$$\text{IMF}_j(t) = \frac{1}{N}\sum_{n=1}^{N} \text{IMF}_j^n(t). \tag{7}$$

d) The residual is updated:

$$r_j(t) = r_{j-1}(t) - \text{IMF}_j(t). \tag{8}$$

6) The iteration stops when the residual $r_j(t)$ is a monotonic function or meets a predefined stopping condition, such as the residual energy falling below a certain threshold. Finally, the original signal $x(t)$ is decomposed as:

$$x(t) = \sum_{j=1}^{J} \text{IMF}_j(t) + r_J(t). \tag{9}$$

B. Kurtosis Value Detection

After decomposing the vibration signal using the CEEMDAN algorithm, obtain a range of IMFs: $\{\text{IMF}_1(t), \text{IMF}_2(t) \cdot \cdot \cdot \text{IMF}_J(t)\}$ and a residual. To identify the IMF containing the main impact components, kurtosis is a statistical measure describing the shape of a probability distribution, indicating the steepness or flatness of the data distribution [23]. It reflects the thickness of the distribution's tails relative to a normal distribution. Higher kurtosis indicates thicker tails and a higher probability of extreme values, while lower kurtosis indicates thinner tails and more concentrated data. Mathematically, for the dataset $\{\text{IMF}_1(t), \text{IMF}_2(t) \cdots \text{IMF}_J(t)\}$, the kurtosis is calculated as:

$$K = \frac{\frac{1}{J}\sum_{j=1}^{J}(\text{IMF}_j(t) - \overline{\text{IMF}}(t))^4}{(\frac{1}{J}\sum_{j=1}^{J}(\text{IMF}_j(t) - \overline{\text{IMF}}(t))^2)^2}, \tag{10}$$

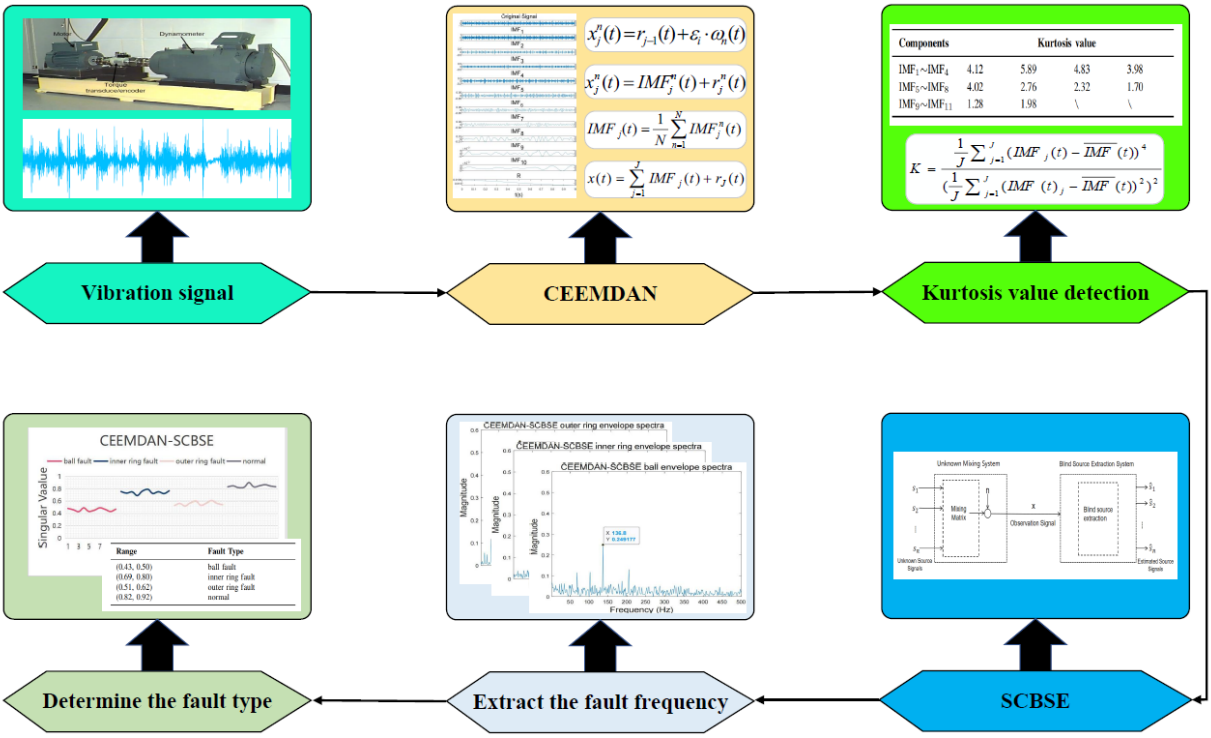

Fig. 1. The flowchart of the proposed CEEMDAN-SCBSE.

where $\overline{\text{IMF}}(t)$ is the mean of the data. The kurtosis indicator is highly sensitive to impulsive components in the signal.

Kurtosis index technology mainly refers to the use of the statistical feature of signal Kurtosis to detect and identify impulsive components caused by local damage in mechanical equipment. Under normal conditions, its value should be around 3. If the value is greater than or equal to 4, it indicates the presence of fault, which are considered vibration impact signals. After calculating the kurtosis values of all the IMFs, the one with the largest kurtosis value is used as the vibration impact signal, which contains the main vibration impact components. Then, calculate its envelope spectrum and determine the IMF for diagnosis by observing the significance of the characteristic frequency of bearing faults.

C. Single-Channel Blind Source Extraction

BSE is a signal processing technique that aims to extract the source of interest from the mixed signals with no prior information of the mixing process. The flowchart of SCBSE is shown in Fig 2. It can achieve the extraction of the source of interest and noise reduction under extremely harsh noise conditions.

Becasuse the influence of equipment and environmental noises in actual environments, the collected faulty bearing signals are mixed with noises. To extract fault signals while eliminating the noise, calculating the kurtosis value of each IMF and select the signal with the highest kurtosis value as the vibration impact signal. The main vibration impact component is extracted while removing the residual noises by using SCBSE technology. The SCBSE is modeled as

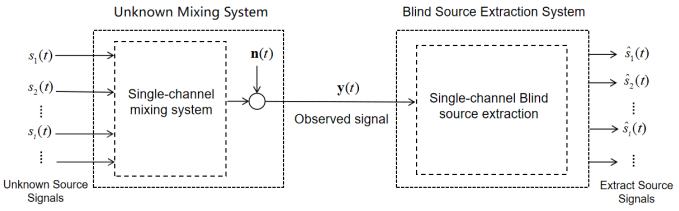

Fig. 2. Flowchart of the SCBSE framework, outlining the blind extraction of fault features from a single noisy signal through iterative optimization of an extraction vector.

$$\boldsymbol{y}(t) = \sum a_i s_i(t) + \boldsymbol{n}(t), \tag{11}$$

where $\boldsymbol{y}(t)$ is the single-channel mixing signal, s_i is the vibration impact signal, and a_i is the mixing matrix coefficient. To extract the source of interest, we design an extraction vector $\boldsymbol{w}$ such that

$$\hat{s}(t) = \boldsymbol{w} \cdot \boldsymbol{y}(t). \tag{12}$$

Then, using the short-time Fourier transform (STFT), Equation (12) is represented as

$$\hat{s}_{fk} = \boldsymbol{w}_f \cdot \boldsymbol{y}_{fk}, \tag{13}$$

where f is the index of the frequency bins, and k is the index of the time frames. $\boldsymbol{w}_f$ and $\boldsymbol{y}_{fk}$ are STFT of $\boldsymbol{w}$ and $\boldsymbol{y}(t)$, respectively. The update rule of $\boldsymbol{w}_f$ is as

$$\boldsymbol{w}_f \leftarrow \mathrm{E}\left[G'\left(\sqrt{\sum_f |\hat{s}_{fk}^0|^2}\right) + |\hat{s}_{fk}^0|^2 G''\left(\sqrt{\sum_f |\hat{s}_{fk}^0|^2}\right)\right]\boldsymbol{w}_f^0 - \mathrm{E}\left[(\hat{s}_{fk}^0)^* G'\left(\sqrt{\sum_f |\hat{s}_{fk}^0|^2}\right)\boldsymbol{y}_{fk}\right] + 2\frac{\partial}{\partial(\boldsymbol{w}_f^*)}\sum_f \log \mid \det(\mathrm{mat}(\boldsymbol{w}_f^0)), \tag{14}$$

where $\mathrm{E}[\cdot]$ is the expectation operator, $G(\cdot) = -\log \hat{f}_s(\cdot)$ with $\hat{f}_s(\cdot) \propto e^{-\sqrt{2(2F+1)}\|\cdot\|_2}$, F is the number of frequency points. $\hat{s}_{fk}^0 = \boldsymbol{w}_f^0 \boldsymbol{y}_{fk}$, 'det$(\cdot)$' is the determinant operation, 'mat$(\cdot)$' is the matrixization operation of vectors, and $(\cdot)^*$ is the complex conjugate operator. The extraction vector $\boldsymbol{w}$ is obtained using the Newton gradient descent, and the source of interest is extracted using Equation (12). Thus, the SCBSE technology can be used to extract the characteristics of bearing faults and significantly reduce noise.

D. Fault Detection and Diagnosis

Hilbert envelope spectrum and singular value entropy are the evaluation indices to validate the feasibility. The fault frequency is extracted using the Hilbert envelope spectrum, and the fault type is determined using singular value entropy.

*1) **Hilbert envelope spectrum**:* By applying a 90^0 phase shift to the original signal, the Hilbert transform enables the construction of an analytic signal in conjunction with the original. The low-frequency modulated signal can be demodulated by obtaining the instantaneous, phase, and amplitude through the analytic signal's modulus [24]. Performing a Hilbert transform on a real signal yields an analytic signal. Then, the envelope signal is obtained by calculating and analyzing the envelope of the signal. Finally, it is subjected to a Fourier transform to result in the Hilbert envelope spectrum because the Hilbert spectrum can effectively demodulate low-frequency modulation signals, and accurate fault location can be achieved through Hilbert envelope spectrum analysis.

*2) **Singular value entropy**:* Singular value entropy is a mathematical tool that combines information entropy and singular value decomposition to quantify the complexity and orderliness of signal structures. According to the principle of information entropy, the entropy algorithm measures data uncertainty or chaos to enable effective data processing and analysis. Singular values, as inherent characteristics of a matrix, serve as indicators of its stability. When faults occur in rolling bearings, the singular values change accordingly. To quantitatively describe the extent of these changes in the operational state, singular value entropy is used to measure the influence of different pulse components on rolling bearings, which quantifies fault features across frequency bands over time [25]. The variation in this entropy across bands reflects the fault characteristics under different operational conditions, making it an effective criterion for assessing bearing health and providing an intuitive diagnostic indicator.

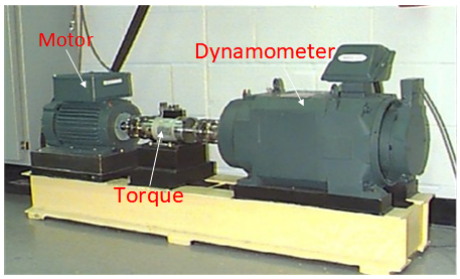

Fig. 3. CWRU test stand of the rolling bearing.

III. Experiments

The superiority ability of the CEEMDAN-SCBSE algorithm are evaluated based on two datasets, including the Case Western Reserve University (CWRU) bearing dataset [26] and the Shenyang Aero-Engine Design and Research Institute (SADRI) rotor-rolling bearing dataset [27].

A. Fault Diagnosis based on the CWRU Dataset

1) Dataset description: The test data is from the CWRU standard bearing fault data [26], the CWRU test stand is shown in Fig. 3. The experimental platform employs a 2-horsepower Reliance Electric motor equipped with SKF6205-2SR deep-groove ball bearings. To capture vibration data from faulty bearings, accelerometers were deployed at both the fan and drive ends of the motor. The bearing speed is 1,797 rpm, the frequency of collected vibration signals is 12 kHz, and the time is 1 s. The bearing data includes four types: ball, inner ring, outer ring, and normal. They are damaged by electrical discharge machining with diameters of 0.3556, 0.5334, and 0.1778 millimeters, respectively. The fault frequencies are 136.4 Hz, 159.3 Hz, and 106.6 Hz, respectively.

2) Results and analysis: Taking the inner ring signal as an example, 10 IMFs components and one residual are obtained using the CEEMDAN, seen in Fig. 4. Some IMFs mainly contain noise components unrelated to fault features. Fault signals typically include high-frequency impact components, and the kurtosis values of the IMFs are obtained using the kurtosis criterion. They are tabulated in Table I, which shows that the kurtosis values of IMF_1, IMF_2, IMF_3, and IMF_5 are all greater than 4, indicating that most of the impact components are retained in these components and are constructed as vibration impact signals. Then, the SCBSE technology is used to extract the main vibration impact component while removing the residual noises. Finally, perform envelope analysis on the extracted vibration impact signal to obtain the envelope spectrum. The same procedure is also applied to the ball and the outer ring fault signal, and their envelope spectra are obtained. The results are shown in Fig. 5. It indicates that the identified fault frequency is very close to the theoretically calculated frequency. To compare the superiority of the algorithms, the IMF with the maximum kurtosis value from the fault signals decomposed by EMD, EEMD, and CEEMDAN was selected as the comparative algorithm, and the results are shown in Fig. 5. By using the CEEMDAN-SCBSE, the amplitude of fault frequency is significantly enhanced, which

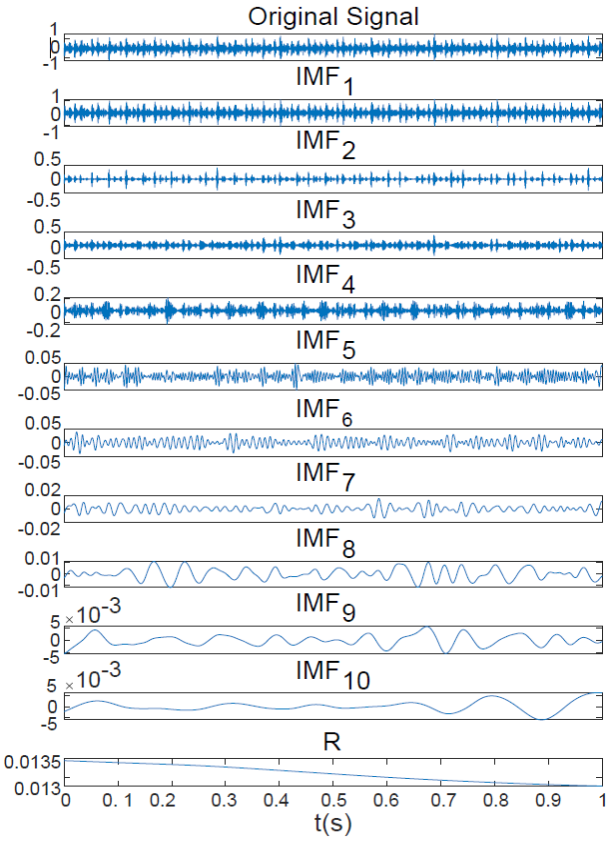

Fig. 4. CEEMDAN decomposition of bearing inner ring signal for CWRU rolling bearing dataset.

TABLE I
IMFs COMPONENT KURTOSIS INDEX OF THE CWRU

Components	Kurtosis value			
$IMF_1 \sim IMF_4$	4.12	5.89	4.83	3.98
$IMF_5 \sim IMF_8$	4.02	2.76	2.32	1.70
$IMF_9 \sim IMF_{11}$	1.28	1.98	\	\

helps to identify fault frequency more accurately. In contrast, fault signals that have not undergone blind extraction exhibit lower amplitude values at the correct fault frequency, making it difficult to determine the fault type accurately.

Then, 10 sets of samples are randomly selected from each of the four vibration signals of bearings, and the singular value entropy of these signals is calculated. Fault classification is performed in Fig. 6. The results reveal a distinct difference in singular value entropy containing fault information obtained from different signal decompositions using EMD, EEMD and CEEMDAN are minimal, resulting in a fuzzy range of singular value entropy values for the four states of bearings, making it challenging to distinguish fault categories. In contrast, the singular value entropy values for the same fault type are closely clustered using the CEEMDAN-SCBSE, and there are significant differences in singular value entropy between different fault categories of rolling bearings, verifying that the CEEMDAN-SCBSE can more accurately identify the fault categories of bearings. In addition, the four states of bearings each belong to a range, and the category ranges do not intersect, as shown in Table II. This indicates that the CEEMDAN-SCBSE can accurately distinguish the fault categories of bearings and achieve precise diagnosis of bearing faults.

TABLE II
CWRU ROLLING BEARING SINGULAR VALUE ENTROPY FAULT INTERVAL

Range	Fault Type
(0.43, 0.50)	ball fault
(0.69, 0.80)	inner ring fault
(0.51, 0.62)	outer ring fault
(0.82, 0.92)	normal

B. Fault Diagnosis based on the SADRI Dataset

1) Dataset Description: The rotor-rolling bearing tester was seen in Fig. 7. It primarily consists of a mounting frame, an electric motor, a base platform, and a gear transmission system. The bearings at both ends of the shaft are of the HRB6304 type. The frequency is 10 kHz, and the duration is 1 s. The rotor-rolling bearing data includes four types: ball, inner ring, outer ring, and normal. They are damaged by electrical discharge wire cutting with diameters of 1.0, 0.6, and 0.6 millimeters, respectively. The fault frequencies are 58.5 Hz, 136.6 Hz, and 88.75 Hz, respectively.

2) Results and Analysis: Taking the outer ring fault as an example, 10 IMFs components and one residual are obtained, as illustrated in Fig. 8. The kurtosis of each IMF is then calculated, and the results are tabulated in Table III, which indicates that IMF_2 possesses the most significant kurtosis value and therefore contains the most pronounced impulsive components. To further extract fault-related features and suppress noises, the remaining IMFs are divided into two groups based on Kurtosis values greater than or less than 4, and combined with IMF_2 to construct a three-channel virtual mixed signal. Subsequently, the SCBSE method is applied to the virtual mixed signals for feature extraction and source separation. Then, perform envelope spectrum analysis on the extracted vibration impact signal to obtain the envelope spectrum. Similarly, the same procedure is also applicable to ball and inner ring fault signals, and their envelope spectra are obtained. The corresponding results are shown in Fig. 9. The envelope spectrum is a core technology that converts high-frequency resonance signals into low-frequency fault characteristic spectra, thereby transforming vibration impact signals that are difficult to visually identify in the time domain into clear fault characteristic frequencies in the frequency domain. The experimental findings reveal that the detected fault frequency agrees well with the theoretical value, and the amplitude of the fault frequency is significantly enhanced after processing, thereby facilitating more accurate fault detection.

To demonstrate the effect of fault diagnosis, 10 sets of samples are randomly selected from each of the four vibration signals to calculate the singular value entropy. The fault identification results are shown in Fig. 10. The singular value entropy of rotor-rolling bearings varies significantly among different fault categories. Compared to EMD, EEMD and CEEMDAN, it can more clearly distinguish fault categories.

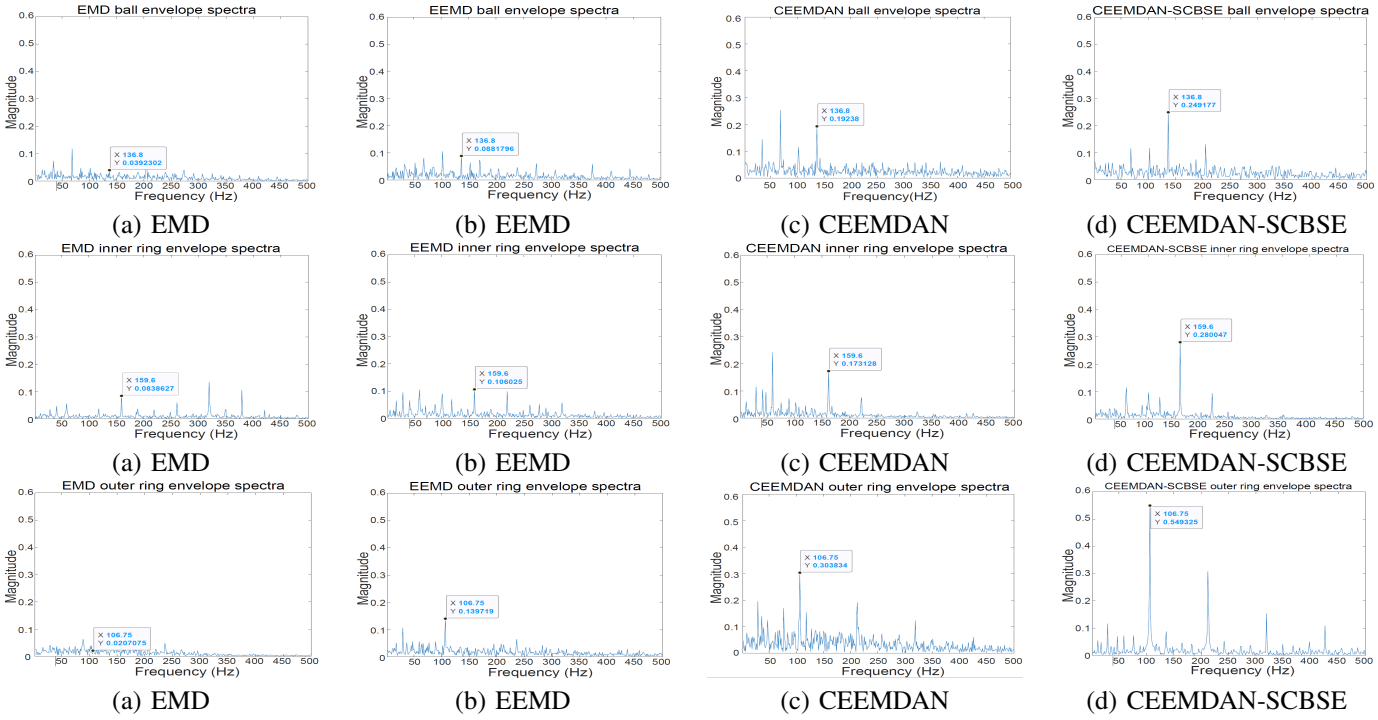

Fig. 5. Envelope spectrum of IMF components for the CWRU dataset decomposed by (a) EMD, (b) EEMD, (c) CEEMDAN, and (d) CEEMDAN-SCBSE. Among them, the first, second, and third rows represent the ball fault, inner ring fault, and outer ring fault, respectively.

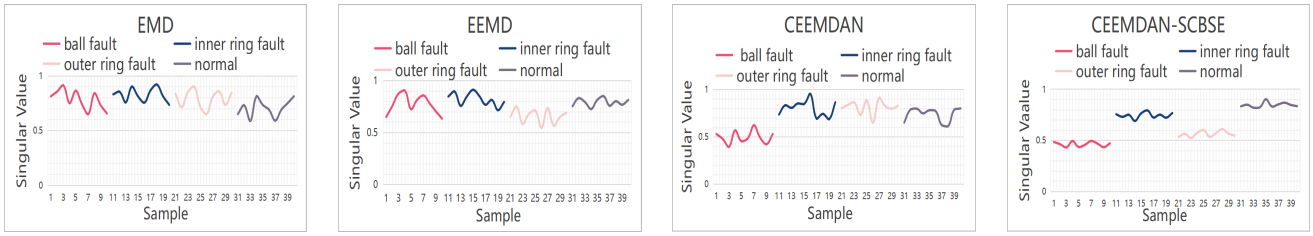

Fig. 6. CWRU rolling bearing singular value entropy fault identification results based on (a) EMD, (b) EEMD, (c) CEEMDAN, and (d) CEEMDAN-SCBSE.

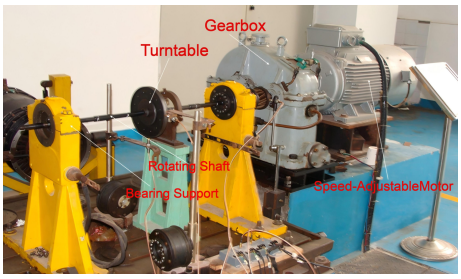

Fig. 7. Physical image of the SADRI test rig.

TABLE III
IMFs COMPONENT KURTOSIS INDEX OF THE SADRI

Components	Kurtosis value			
$IMF_1 \sim IMF_4$	7.85	11.02	5.92	4.13
$IMF_5 \sim IMF_8$	4.41	3.31	3.73	3.34
$IMF_9 \sim IMF_{10}$	1.87	3.59	\	\

TABLE IV
SADRI ROTOR-ROLLING BEARING SINGULAR VALUE ENTROPY FAULT INTERVAL

Range	Fault Type
(0.77, 0.83)	ball fault
(0.88, 0.92)	inner ring fault
(0.83, 0.88)	outer ring fault
(0.92, 0.97)	normal

Additionally, the four states of the rotor-rolling bearing each belong to an interval, and there is no intersection between the categories, seen in Table IV. The fault categories are accurately distinguished, thereby achieving precise diagnosis.

C. Noise Reduction Evaluation Results and Analysis

The noise reduction performance of the algorithms is evaluated using three evaluation indices, i.e., the kurtosis value (K), measured in dimensionless units, signal-to-noise ratio (SNR), measured in decibels (dB), and root mean square

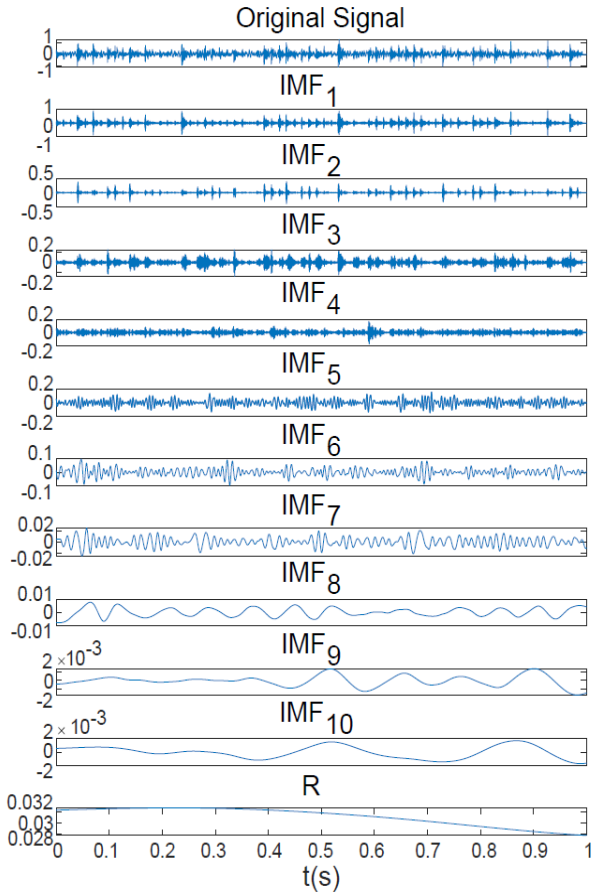

Fig. 8. CEEMDAN decomposition of bearing outer ring signal for SADRI rotor-rolling bearing dataset.

error (RMSE), measured in millimeters (mm) [29], [30]. The definition of the kurtosis value is seen in Equation (12), the bigger the K value, the better the noise reduction. The SNR reflects the denoising capability, and the RMSE quantifies the deviation between the original signal and its reconstructed version, serving as a metric of their discrepancy. An enhanced SNR and a reduced RMSE collectively indicate a more effective noise suppression performance.

The comparison results of the three evaluation indices for noise reduction analysis are tabular in Table V. The kurtosis values and SNRs of the noise-reduced signals obtained by the CEEMDAN-SCBSE are both greater than those of the EMD, EEMD and CEEMDAN, and the RMSE are reduced. Taking the CEEMDAN and CEEMDAN-SCBSE as an example, in the CWRU bearing dataset, the kurtosis value and SNR have increased by 24.28% and 53.35%, respectively. The RMSE has decreased by 10.86%. In the SADRI rotor-rolling bearing dataset, the kurtosis value and SNR have increased by 41.74% and 28.57%, respectively. The RMSE has decreased by 4.13%. In different bearing datasets, kurtosis values and SNR indicators show varying degrees of improvement, while RMSE decreased, confirming the superiority ability of the CEEMDAN-SCBSE algorithm. In sum, the CEEMDAN-SCBSE algorithm significantly mitigates the problem of noise reduction and provides a substantial improvement in SNR and RMSE.

TABLE V
COMPARISON OF THE THREE EVALUATION INDICES FOR NOISE REDUCTION ANALYSIS BASED ON THE BEARING DATASETS

Index	**CWRU bearing dataset**			
	EMD	EEMD	CEEMDAN	CEEMDAN-SCBSE
K	5.49	6.52	5.89	**7.32**
SNR(dB)	35.52	40.69	42.83	**65.68**
RMSE(mm)	0.0479	0.0402	0.0350	**0.0312**
Index	**SADRI rotor-rolling bearing dataset**			
	EMD	EEMD	CEEMDAN	CEEMDAN-SCBSE
K	9.48	9.79	11.02	**15.62**
SNR(dB)	32.08	34.61	39.73	**51.08**
RMSE(mm)	0.125	0.134	0.0921	**0.0883**

IV. CONCLUSIONS

This paper proposed a CEEMDAN-based single-channel blind extraction method for bearing fault detection and diagnosis, facilitating accurate identification of fault features and eliminating noise interference. Validated on public CWRU and SADRI datasets, the CEEMDAN-SCBSE algorithm outperforms the standard CEEMDAN, achieving superior performance in kurtosis, SNR, and RMSE. Specifically, it attains a maximum kurtosis of 15.62, highlighting impact components; a peak SNR of 65.68 dB; and a minimal RMSE of 0.0312 mm, demonstrating strong noise suppression while retaining critical fault features. It confirms the powerful denoising capability of the CEEMDAN-SCBSE method. Additionally, the proposed algorithm constructed a comprehensive automated diagnostic chain, spanning from signal denoising to state evaluation, and subsequently to fault localization and diagnosis, thereby providing a systematic approach for handling bearing fault problems and a core algorithm framework for developing universal, platform-based intelligent diagnostic software, which will be helpful for practical industrial applications.

Future efforts will focus on enhancing the proposed algorithm to address fault detection and diagnosis in variable operating environments, as well as the prediction of remaining bearing life. Meta learning and multi-source information fusion techniques are popular algorithms for solving this type of problem. In future work, we will integrate them into our algorithm framework to achieve better applications.

REFERENCES

[1] X. Q. Wu, H. Wang, J. Meng, L. Zhang, C. Chen, and W. Wang. “Collaboration transfer enabled standard rank control chart for cross-domain incipient fault detection of bearings with limited historical data”, IEEE Transactions on Instrumentation and Measurement, vol. 74, p. 3546812, 2025. doi: 10.1109/TIM.2025.3582306.

[2] A. Menendez, L. Magadan, J. C. Granda Candas, and F. J. Suarez Alonso. “Fault detection system for bearings in electric motors using variational auto encoders”, IEEE Latin America Transactions, vol. 23, no. 5, pp. 371–379, 2025. doi: 10.1109/TLA.2025.10974368.

[3] Y. K. Deng, S. H. Tang, S. Chang, H. Zhang, D. C. Liu, and W. Wang. “A novel scheme for range ambiguity suppression of spaceborne sar based on underdetermined blind source separation”, IEEE Transactions on Geoscience and Remote Sensing, vol. 63, p. 5207915, 2025. doi: 10.1109/TGRS.2025.3556296.

[4] Y. Xie, T. Zou, J. J. Yang, W. J. Sun, and S. L. Xie. “SA-UCBSS: Sparsity-based adaptive underdetermined convolutive blind source separation”, Knowledge-Based Systems, vol. 300, p. 112224, 2024. doi: 10.1016/j.knosys.2024.112224.

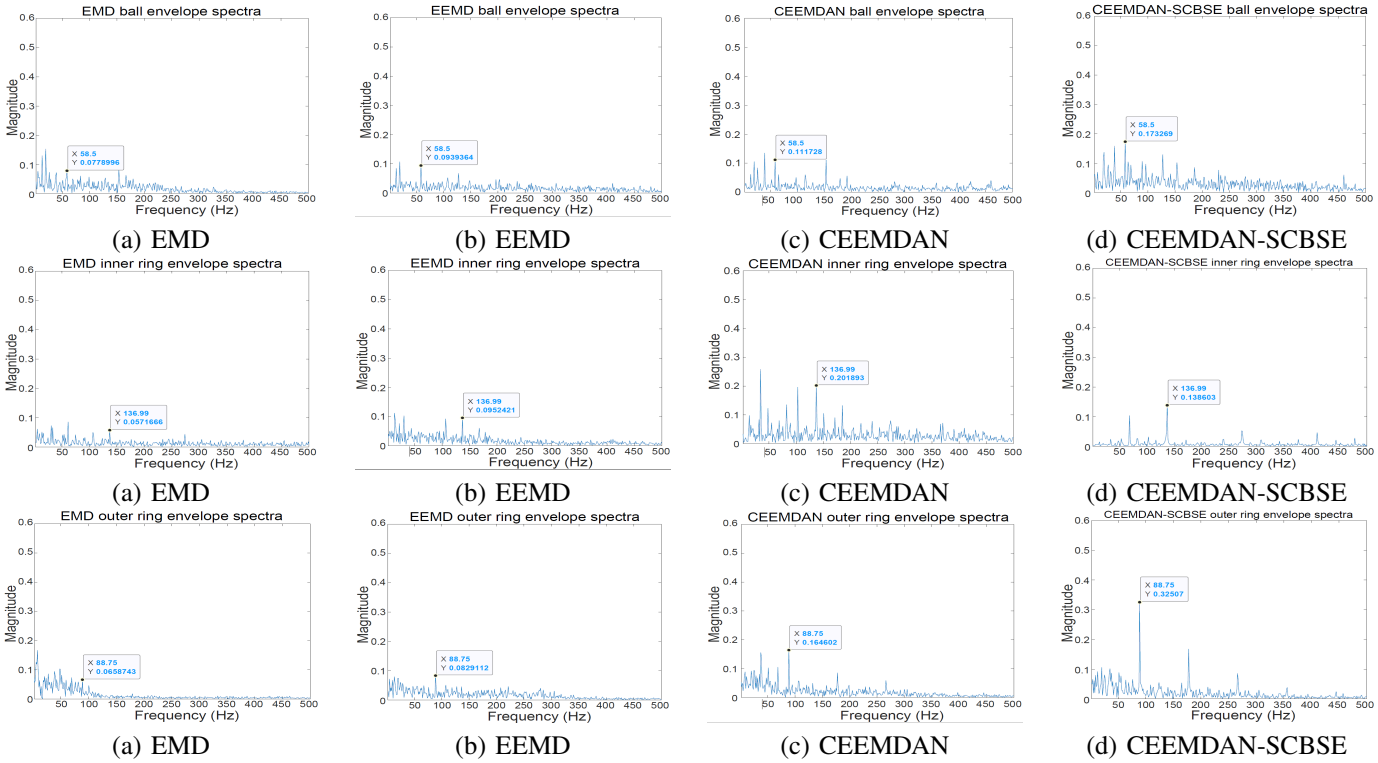

Fig. 9. Envelope spectrum of IMF components for the SADRI rotor-rolling bearing dataset decomposed by (a) EMD, (b) EEMD, (c) CEEMDAN, and (d) CEEMDAN-SCBSE. Among them, the first, second, and third rows represent the ball fault, inner ring fault, and outer ring fault, respectively.

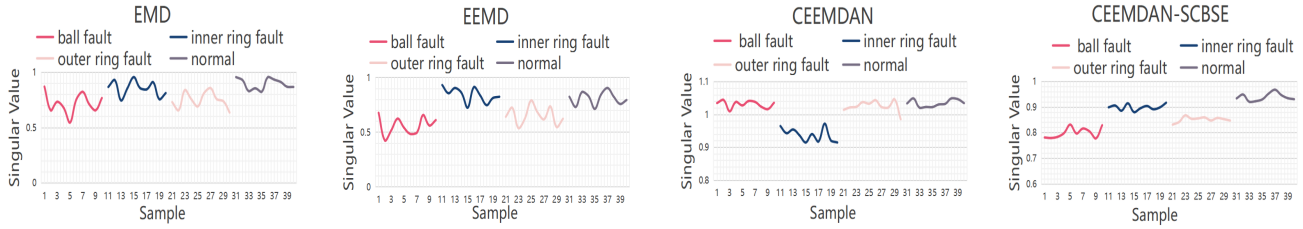

Fig. 10. SADRI rotor-rolling bearing singular value entropy fault identification results based on (a) EMD, (b) EEMD, (c) CEEMDAN, (d) CEEMDAN-SCBSE.

[5] H. X. Ruan, S. Zhao, Z. B. Lin, and J. Lu. "Computationally-efficient blind source extraction under extremely low SNR conditions based on principal component analysis", Applied Acoustics, vol. 236, p. 110709, 2025. doi: 10.1016/j.apacoust.2025.110709.

[6] Z. Koldovsky, J. Cmejla, and S. O'Regan. "Blind capon beamformer based on independent component extraction: Single-parameter algorithm", IEEE Signal Processing Letters, vol. 32, pp. 801–805, 2025. doi: 10.1109/LSP.2025.3538261.

[7] X. Zhao, Y. Qin, C. He, and L. Jia. "Underdetermined blind source extraction of early vehicle bearing faults based on EMD and kernelized correlation maximization", Journal of Intelligent Manufacturing, vol. 33, pp. 185–201, 2020. doi: 10.1007/s10845-020-01655-1.

[8] K. W. Wang, Q. S. Hao, X. Zhang, Z. Y. Tang, and Y. Shen. "Blind source extraction of acoustic emission signals for rail cracks based on ensemble empirical mode decomposition and constrained independent component analysis", Measurement, vol. 157, p. 107653, 2020. doi: 10.1016/j.measurement.2020.107653.

[9] T. Thelaidjia, N. Chetih, A. Moussaoui, and S. Chenikher. "Successive variational mode decomposition and blind source separation based on salp swarm optimization for bearing fault diagnosis", The International Journal of Advanced Manufacturing Technology, vol. 125, pp. 5541–5556, 2023. doi: 10.1007/s00170-023-10968-3.

[10] R. K. Mandal, H. Devarajan, S. Nandi, T. B. Shanker, and M. Ghassemi. "An underdetermined single-channel blind-source-separation for multisource acoustic-emission-based partial discharge signals in power transformers", IEEE Transactions on Plasma Science, vol. 53, no. 4, pp. 788–797, 2025. doi: 10.1109/TPS.2025.3538746.

[11] X. Y. Jia, M. Zhang, Y. Z. Gao, and Y. N. Guo. "Transition-PDualGAN: An enhanced framework for single-channel blind source separation with transition domain", Digital Signal Processing, vol. 160, p. 105037, 2025. doi: 10.1016/j.dsp.2025.105037.

[12] N. E. Huang. "The empirical mode decomposition and the hilbert spectrum for nonlinear and non-stationary time series analysis", Proceedings of Royal Society of London, vol. 545, no. 1971, pp. 903–995, 1998. doi: 10.1098/rspa.1998.0193.

[13] D. G. Li, X. Y. Luo, J. M. Zhao, F. M. Wu, H. R. Jiang, and D. Y. Shi. "GNSS signal-to-noise snow depth inversion based on robust empirical mode decomposition", Intelligent and Converged Networks, vol. 6, no. 2, pp. 115–128, 2025. doi: 10.23919/ICN.2025.0007.

[14] Y. P. Wang, Q. S. Zhang, R. F. Cao, S. Zhang, S. S. Li, and D. Xu. "The single-channel blind source separation based on VMD and Tukey M estimation for rolling bearing composite fault diagnosis", Measurement and Control, vol. 56, no. 9/10, pp. 1599–1612, 2023. doi: 10.1177/00202940231174405.

[15] J. R. Yeh, J. S. Shieh, and N. E. Huang. "Complementary ensemble empirical mode decomposition: a novel noise enhanced data analysis

method", Advances in Adaptive Data Analysis, vol. 2, no. 2, pp. 135–156, 2010. doi: 10.1142/S1793536910000422.
[16] A. Humeau-Heurtier, G. Mahe, and P. Abraham. "Multi-dimensional complete ensemble empirical mode decomposition with adaptive noise applied to laser speckle contrast images", IEEE Transactions on Medical Imaging, vol. 34, no. 10, pp. 2103–2117, 2015. doi: 10.1109/TMI.2015.2419711.
[17] M. A. Colominas, G. Schlotthauer, and M. E. Torres. "Improved complete ensemble EMD: A suitable tool for biomedical signal processing", Biomedical Signal Processing and Control, vol. 14, pp. 19–29, 2014. doi: 10.1016/j.bspc.2014.06.009.
[18] Q. W. Li, X. Xiao, L. Wang, H. Song, H. Kono, P. F. Liu, H. Lu, and T. Kikkawa. "Direct extraction of tumor response based on ensemble empirical mode decomposition for image reconstruction of early breast cancer detection by UWB", IEEE Transactions on Biomedical Circuits and Systems, vol. 9, no. 5, pp. 710–724, 2015. doi: 10.1109/TBCAS.2015.2481940.
[19] Z. W. Zhuang, H. Y. Chen, J. X. Tang, M. S. Chen, and X. J. Hezhou. "A new denoising method for ship-radiated noise based on complete ensemble empirical mode decomposition", 2025 IEEE 8th Information Technology and Mechatronics Engineering Conference (ITOEC), vol. 8, pp. 1638–1642, 2025. doi: 10.1109/ITOEC63606.2025.10967791.
[20] Z. Pan, B. Xu, W. J. Chen, D. Fan, X. H. Meng, M. F. Peng, and C. Zhou. "Improved complete ensemble empirical mode decomposition with adaptive noise and its application in noise reduction for fiber optic sensing", Journal of Lightwave Technology, vol. 43, no. 5, pp. 2466–2474, 2025. doi: 10.1109/JLT.2024.3489953.
[21] R. Abdelkader, A. Kaddour, A. Bendiabdellah, and Z. Derouiche. "Rolling bearing fault diagnosis based on an improved denoising method using the complete ensemble empirical mode decomposition and the optimized thresholding operation", IEEE Sensors Journal, vol. 18, no. 17, pp. 7166–7172, 2018. doi: 10.1109/JSEN.2018.2853136.
[22] Y. Li, J. W. Zhou, H. G. Li, G. Meng, and J. Bian. "A fast and adaptive empirical mode decomposition method and its application in rolling bearing fault diagnosis", IEEE Sensors Journal, vol. 23, no. 1, pp. 567–576, 2023. doi: 10.1109/JSEN.2022.3223980.
[23] S. Misra, R. D. De Roo, and C. S. Ruf. "Sensitivity of the kurtosis statistic as a detector of pulsed sinusoidal RFI", IEEE Transactions on Geoscience and Remote Sensing, vol. 45, no. 7, pp. 1938–1946, 2007. doi: 10.1109/TGRS.2006.888101.
[24] L. He, X. L. Li, Q. Y. Zhou, C. Yi, and Y. F. Li. "Neural network integrated with classical signal processing techniques for generating optimized square envelope spectrum and its application in machine condition monitoring", IEEE Transactions on Instrumentation and Measurement, vol. 74, p. 3548311, 2025. doi: 10.1109/TIM.2025.3584118.
[25] S. Chen, Y. Lin, Y. Yuan, X. X. Li, L. S. Hou, and S. N. Zhang. "Suppressive interference suppression for airborne sar using bss for singular value and eigenvalue decomposition based on information entropy", IEEE Transactions on Geoscience and Remote Sensing, vol. 61, p. 5205611, 2023. doi: 10.1109/TGRS.2023.3263218.
[26] The bearing date center website of Case Western Reserve University. [Online]. Available: http://csegroups.case.edu/bearingdatacenter/pages/download-data-file.
[27] The rotor-rolling bearing dataset of Shenyang Aero-Engine Design and Research Institute. [Online]. Available: http://ides.nuaa.edu.cn.
[28] S. Y. Shao, S. McAleer, R. Q. Yan, and P. Baldi. "Highly accurate machine fault diagnosis using deep transfer learning", IEEE Transactions on Industrial Informatics, vol. 15, no. 4, pp. 2446–2455, 2019. doi: 10.1109/TII.2018.2864759.
[29] X. L. Liu, M. Z. Jiang, Z. Q. Liu, and H. Wang. "A morphology filter-assisted extreme-point symmetric mode decomposition (MF-ESMD) denoising method for bridge dynamic deflection based on ground-based microwave interferometry", Shock and Vibration, vol. 2020, no. 11, pp. 1–13, 2020. doi: 10.1155/2020/8430986.
[30] X. L. Liu, H. Wang, and Y. M. Huang. "SCBSS signal de-noising method of integrating EEMD and ESMD for dynamic deflection of bridges using GBSAR", IEEE Journal of Selected Topics in Applied Earth Observations and Remote Sensing, vol. 14, pp. 2845–2856, 2021. doi: 10.1109/JSTARS.2021.3061543.

Yuan Xie received the Ph.D. degree in control science and engineering from Guangdong University of Technology in 2019. He is currently a Lecturer with the School of Mechanical and Electrical Engineering at Guangzhou University. His research interests include blind signal separation, intelligent detection, and machine learning. He has authored over 20 SCI journal papers and holds 9 patents. He has led research projects including the National Natural Science Foundation of China Youth Project and the Guangzhou Basic Research Program.

Zhangchi Wei received the B.Eng. degree from Guangzhou University, Guangzhou, China, in 2023. He is currently pursuing the M.Eng. degree in control engineering with Guangzhou University, Guangzhou, China. His current research interests include fault detection, blind signal separation, and deep learning.

Jinshi Yu received the Ph.D. in Control Science and Engineering from Guangdong University of Technology in 2020. He served as a postdoctoral researcher at Guangzhou University from 2021 to 2023. His research focuses on tensor decomposition-based image completion, denoising, background removal, and clustering. He has published over 10 high-level academic papers and has led one National Natural Science Foundation Youth Project, in addition to participating in two other NSFC projects.

Yifei Sun received the Ph.D. degree from the School of Computer Science, Guangdong University of Technology in 2025. He is currently pursuing postdoctoral research with the School of Cyber Space Institute of Advance Technology at Guangzhou University. His research interests include edge computing,intelligent detection and deep learning.

Zhipeng Chen received the Ph.D. degree from Sun Yat-sen University in 2019. From 2019 to 2022, he conducted postdoctoral research at Sun Yat-sen University. His main research interests include functional microstructure fabrication, magnetic materials, and robotics applications. He has published papers in journals such as Nature Communications and Matter, and has led research projects including the National Youth Science Foundation. His recent work focuses on microstructure fabrication, intelligent detection, and stochastic processes.